

# Novel bright blue emissions IIB group complexes constructed with various polyhedron-induced 2-[2'-(6-methoxy-pyridyl)]-benzimidazole derivatives†

Shuo Chen, Rui-Qing Fan,\* Xin-Ming Wang and Yu-Lin Yang\*

 Cite this: *CrystEngComm*, 2014, 16, 6114

Five IIB group complexes,  $[ZnL^1Cl_2]$  (1),  $\{[CdL^1Cl_2]\}_2$  (2),  $[Cd(L^1)_2(NO_3)_2] \cdot H_2O$  (3),  $[HgL^1Cl_2]$  (4), and  $[ZnL^2Cl_2]$  (5) [ $L^1 = 1$ -[2-(6-methoxy-2-pyridylmethyl)]-2-[2-(6-methoxy-pyridyl)]benzimidazole;  $L^2 = 2$ -[2-(6-methoxypyridyl)]benzimidazole] have been synthesized and structurally characterized by elemental analysis, IR spectroscopy,  $^1H$  NMR,  $^{13}C$  NMR and X-ray single-crystal analyses. The structural investigations testify that the ionic radius and counterions ( $Cl^-$  and  $NO_3^-$ ) cooperatively affect the coordination mode of central metal. As small and medium radii, four-coordinated  $Zn^{2+}$  (1 and 5) and five-coordinated  $Cd^{2+}$  (2) possess tetrahedron and trigonal bipyramid geometries, respectively. Though  $Hg^{2+}$  (4) has a larger radius, its three-coordinated geometry is trigonal planar in order to eliminate repulsive forces. Further observations illustrate that  $Cd^{2+}$  (3) is bound to two ligands  $L^1$  when  $NO_3^-$  is the counter anion, forming seven-coordinated monocapped trigonal prismatic geometry. Complexes 1–5 display bright blue luminescence with the emission maxima ( $\lambda_{max}$ ) ranging from 399 to 499 nm at 298 K, depending on the  $N,N'$ -chelating ligand-centered  $\pi^* \rightarrow \pi$  transition. Upon cooling to 77 K, the complexes show rich structured emission profiles compared to those at 298 K. The emission lifetimes of L and 1–5 are on the microsecond scale. The emission efficiency of 1–5 is shown by quantum yields ranging from 0.23 to 0.40. Complexes 1–5 offer a good insight into the opportunities in the utilization of blue materials for application and function.

 Received 20th February 2014,  
Accepted 7th April 2014

DOI: 10.1039/c4ce00382a

[www.rsc.org/crystengcomm](http://www.rsc.org/crystengcomm)

## Introduction

Over recent decades, rational design and synthesis of functional complexes with desired structures and properties have received increasing attention. In this regard, transition-metal complexes based on benzimidazole derivatives have proven to be promising owing to their potential functions as new classes of materials.<sup>1</sup> As luminescent materials, benzimidazole derivatives have been extensively studied because of their ideal characteristics for highly energy-efficient, flat-panel displays and the next generation of solid-state lighting.<sup>2</sup> In general, the scale of the  $\pi$ -conjugated system for the ligand and the electronic effect of substituents on the ligand are the dominating elements for luminescence properties.<sup>3</sup> Both the bulky aromatic coupling system and appropriate electron-donating or electron-withdrawing substituents on the ligand may facilitate the bathochromic shift of the emission color.<sup>4</sup> Therefore,

it is not an easy task to design blue-emitting ligands with high quantum yield, relatively reasonable cost and a simple reaction procedure. It is well-known that diarylanthracene, di(styryl)arylene, fluorene, pyrene, benzimidazole and their derivatives are excellent blue emitters, as reported in the literature.<sup>5</sup> Among the different ligand candidates, the deprotonated benzimidazole ligand is an excellent blue emitter when bonded to a central metal atom in a bridging mode.<sup>6</sup> Moreover, based on the inherent character of the benzimidazole group, deprotonation for the NH group on imidazole can be realized to attach a wide variety of substituents. Benzimidazole allows readily modifying and creating potentially strong  $\pi$ - $\pi$  stacking interactions to form supramolecular structures.<sup>7</sup> A larger  $\pi$  delocalization system is anticipated to enhance the luminescence properties. Besides, these multifunctional benzimidazole derivatives are capable of forming complexes with certain metal ions which can exhibit uncommon antibacterial activity. Their applications in the fields of pesticides and medicine possess high efficiency, broad spectrum and high selectivity.<sup>8</sup>

Motivated by this research trend and our project on the synthesis of functional complexes, the luminescence properties of some benzimidazole derivatives complexes are reported.

Department of Chemistry, Harbin Institute of Technology, Harbin 150001, PR China.  
E-mail: fanruiqing@hit.edu.cn, ylyang@hit.edu.cn; Fax: +86 451 86413710

† Electronic supplementary information (ESI) available. CCDC 938861, 938858, 938859, 933809, 938860 and 946739. For ESI and crystallographic data in CIF or other electronic format see DOI: 10.1039/c4ce00382a

Besides, primary exploration of the antibacterial activity is carried out (Fig. S10, ESI†). Herein, we present the photophysical properties of five IIB group complexes bearing the extended  $\pi$ -conjugated benzimidazole derivatives 1-[2-(6-methoxy-2-pyridylmethyl)]-2-[2-(6-methoxy-pyridyl)]-benzimidazole ( $L^1$ ) and 2-[2-(6-methoxy-pyridyl)]-benzimidazole ( $L^2$ ); both ligands feature two neutral nitrogen donors that can chelate a metal center.  $L^1$  has a larger conjugated  $\pi$ -system than  $L^2$ ; the functional group ( $-\text{CH}_2\text{-Py-OCH}_3$ ) on the NH position of the imidazole ring may play a crucial role in the formation of the complexes and their luminescence properties. To further enhance the rigidity of the chelate, IIB group metal salts with different counterions are successfully employed in the isolation of complexes 1–5. The counterion ( $\text{Cl}^-$  and  $\text{NO}_3^-$ ) and ionic radius are two key parameters for controlling their structural variations.<sup>9</sup> The luminescence behavior of  $L$  and complexes 1–5 is determined in the solid state and solution, which display intense blue emission at 298 K and 77 K. The Commission Internationale de L'Eclairage (CIE) coordinates of the photoluminescence spectra of complexes 1–5 are calculated, which further demonstrates that the color gamut is located in the blue region.

## Experimental section

### Materials and measurements

All reagents were of analytical grade from commercial sources and were used directly without any further purification. 1,2-Diaminobenzene and 6-methoxy-2-pyridinecarboxaldehyde were purchased from Aldrich Co., Ltd and Rui Yi Sci. & Tec. Co. Ltd. (Shanghai, China), respectively. Metal salts were purchased from Ji Nan Henghua Sci. & Tec. Co. Ltd. (Shandong, China). Solvents for reaction and photophysical studies were dried and freshly distilled under dry nitrogen gas before use.  $^1\text{H}$  NMR (400 MHz) and  $^{13}\text{C}$  NMR (100 MHz) spectra were recorded on a Bruker Avance-400 spectrometer using  $\text{Si}(\text{CH}_3)_4$  as an internal standard at room temperature. Elemental analyses for C, H, and N were performed on a Perkin-Elmer 2400 automatic analyzer. Fourier transform (FT)-IR spectra were measured on a Perkin-Elmer Spectrum 100 FT-IR spectrometer with samples prepared as KBr discs. Thermogravimetric analyses were performed on a Perkin-Elmer STA 6000 Simultaneous Thermal Analyzer with a heating rate of  $10\text{ }^\circ\text{C min}^{-1}$  in a flowing air atmosphere. UV-vis spectra were recorded on a Perkin-Elmer Lambda 35 spectrometer. The solid-state and solution photoluminescence analyses were carried out on an Edinburgh FLS920 fluorescence spectrometer in the range of 200–800 nm. The visible detector as well as the lifetime setup was a red-sensitive photomultiplier (type r928). Low temperature analyses were carried out at 77 K with an Oxford Optistat DN™ cryostat (with liquid nitrogen filling). Lifetime studies were performed using a photon-counting system with a microsecond pulse lamp as the excitation source. The emission decays were analyzed by the sum of exponential functions. The decay curve is well fitted into a double exponential function:  $I = I_0 + A_1 \exp(-t/\tau_1) + A_2 \exp(-t/\tau_2)$ , where  $I$  and  $I_0$  are the luminescence intensities at time  $t = t$  and  $t = 0$ , respectively, whereas  $\tau_1$

and  $\tau_2$  are defined as the luminescence lifetimes. The average lifetime was calculated according to the following eqn (1):

$$\frac{\tau_1^2 A_1 \% + \tau_2^2 A_2 \%}{\tau_1 A_1 \% + \tau_2 A_2 \%} \quad (1)$$

The luminescence quantum yields of the complexes were measured in  $\text{CH}_3\text{OH}$  at room temperature and cited relative to a reference solution of quinine sulfate ( $\Phi = 0.546$  in  $0.5\text{ mol dm}^{-3}\text{ H}_2\text{SO}_4$ ) as a standard, and they were calculated according to the well-known eqn (2):<sup>10</sup>

$$\frac{\phi_{\text{overall}}}{\phi_{\text{ref}}} = \left( \frac{n}{n_{\text{ref}}} \right)^2 \frac{A_{\text{ref}}}{A} \frac{I}{I_{\text{ref}}} \quad (2)$$

In eqn (2),  $n$ ,  $A$ , and  $I$  denote the refractive index of solvent, the area of the emission spectrum, and the absorbance at the excitation wavelength, respectively, and  $\phi_{\text{ref}}$  represents the quantum yield of the standard quinine sulfate solution. The subscript 'ref' denotes the reference, and the absence of a subscript implies an unknown sample. For the determination of the quantum yield, the excitation wavelength was chosen so that  $A < 0.05$ .

Synthesis of 1-[2-(6-methoxy-2-pyridylmethyl)]-2-[2-(6-methoxypyridyl)]benzimidazole ( $L^1$ ): a mixture of 1,2-diaminobenzene (1.1 g, 10 mmol) and 6-methoxy-2-pyridinecarboxaldehyde (2.7 g, 20 mmol) was refluxed in anhydrous toluene (20 mL) in the presence of a catalytic amount of formic acid for 24 hours. After the reaction was over, the resulting solution was concentrated under reduced pressure (oil pump) to obtain the yellow solid. The crude product was recrystallized from methanol to give the white block solid. Yield: 1.6 g (45%); UV ( $\text{CH}_3\text{OH}$ ,  $25\text{ }^\circ\text{C}$ ):  $\lambda_{\text{max}}$  (nm) = 232, 279, 319; FT-IR (KBr,  $\text{cm}^{-1}$ ):  $\nu = 3446$  (m), 3050 (m,  $\nu_{\text{Py, C-H}}$ ), 2949 (m), 2860 (w), 1588 (s), 1471 (s), 1442 (s), 1391 (m), 1316 (m), 1266 (m), 1073 (m), 1027 (m), 901 (s), 746 (s), 431 (s);  $^1\text{H}$  NMR (400 MHz,  $\text{DMSO-}d_6$ , ppm):  $\delta = 8.00$  (d, 1H,  $J = 7.2$  Hz, Py- $H$ ), 7.87 (d, 1H,  $J = 7.2$  Hz, Py- $H$ ), 7.77 (dt, 1H,  $J = 3.6, 6.4$  Hz, Py- $H$ ), 7.62 (dt, 1H,  $J = 4.0, 7.2$  Hz, Py- $H$ ), 7.53 (t, 1H,  $J = 8.0$  Hz, Py- $H$ ), 7.28 (dt, 2H,  $J = 3.6, 6.4$  Hz, Py- $H$ , Ph- $H$ ), 6.89 (d, 1H,  $J = 8.0$  Hz, Ph- $H$ ), 6.61 (d, 1H,  $J = 8.4$  Hz, Ph- $H$ ), 6.42 (d, 1H,  $J = 7.2$  Hz, Ph- $H$ ), 6.22 (s, 2H,  $\text{CH}_2$ ), 3.68 (s, 3H,  $\text{OCH}_3$ ), 3.63 (s, 3H,  $\text{OCH}_3$ );  $^{13}\text{C}$  NMR (100 MHz,  $\text{DMSO-}d_6$ , ppm):  $\delta = 162.92, 162.56, 154.83, 149.48, 147.41, 142.00, 139.81, 139.76, 136.77, 123.30, 122.57, 119.49, 117.17, 112.88, 111.01, 110.77, 108.84, 53.12, 52.71, 49.51$ ; elemental analysis calcd for  $L^1$  [ $\text{C}_{20}\text{H}_{18}\text{N}_4\text{O}_2$  (346.38)]: C, 69.35; H, 5.24; N, 16.17%; found: C, 69.58; H, 5.12; N, 16.39%.

Synthesis of 2-[2-(6-methoxy-pyridyl)]-benzimidazole ( $L^2$ ):  $L^2$  was prepared in a similar procedure as that described for  $L^1$ , except using 6-methoxy-2-pyridinecarboxaldehyde (1.4 g, 10 mmol) instead of 6-methoxy-2-pyridinecarboxaldehyde (2.7 g, 20 mmol). After the reaction was over, the resulting solution was concentrated under reduced pressure (oil pump) to obtain a yellow solid. The crude product was recrystallized in ether to give the white block solid. Yield: 1.3 g (60%); UV

(CH<sub>3</sub>OH, 25 °C):  $\lambda_{\max}$  = 228, 268, 307 nm; FT-IR (KBr):  $\nu$  = 3055 (w), 2984 (w,  $\nu_{\text{Py}}$ , C-H), 2946 (m), 1579 (s), 1470 (s), 1415 (s), 1325 (m), 1267 (m), 1149 (m), 1032 (m), 750 (s), 433 (m) cm<sup>-1</sup>; <sup>1</sup>H NMR (400 MHz, DMSO-*d*<sub>6</sub>, 25 °C):  $\delta$  = 12.95 (s, 1H, imidazole-*H*), 8.10 (d, 1H, *J* = 7.2 Hz, Py-*H*), 7.90 (d, 1H, *J* = 8.0 Hz, Py-*H*), 7.74 (t, 1H, *J* = 7.6 Hz, Py-*H*), 7.30 (m, 1H, Ph-*H*), 6.79 (d, 1H, *J* = 8.4 Hz, Ph-*H*), 6.59 (d, 1H, *J* = 8.4 Hz, Ph-*H*), 6.37 (d, 1H, *J* = 7.2 Hz, Ph-*H*), 3.87 (s, 3H, OCH<sub>3</sub>); elemental anal. calcd for L<sup>2</sup> [C<sub>13</sub>H<sub>10</sub>N<sub>3</sub>O (224.24)]: C 69.63; H 4.50; N 18.74%; found: C 69.56; H 4.57; N 18.81%.

#### Preparation of [ZnL<sup>1</sup>Cl<sub>2</sub>] (1)

A solution ZnCl<sub>2</sub> (13.6 mg, 0.1 mmol) in CH<sub>3</sub>CN (10 mL) was added to a solution of L<sup>1</sup> (34.8 mg, 0.1 mmol) in CH<sub>3</sub>CN (10 mL). The mixture was stirred under reflux for 8 hours. After cooling to room temperature, the resulting solution was removed by filtration. The filtrate was kept for evaporation at room temperature for 4 days. Crystals suitable for X-ray structure determination were picked from the solution. Yield: 38.7 mg (80%); UV (CH<sub>3</sub>OH, 25 °C):  $\lambda_{\max}$  (nm) = 239, 279, 318; FT-IR (KBr, cm<sup>-1</sup>):  $\nu$  = 3446 (m), 3086 (w,  $\nu_{\text{Py}}$ , C-H), 2949 (w), 2858 (w), 1605 (s), 1580 (s), 1491 (s), 1465 (s), 1428 (s), 1322 (m), 1151 (m), 1052 (m), 1031 (m), 1024 (m), 795 (m), 755 (m); <sup>1</sup>H NMR (400 MHz, DMSO-*d*<sub>6</sub>, ppm):  $\delta$  = 7.99 (d, 1H, *J* = 7.6 Hz, Py-*H*), 7.84 (t, 1H, *J* = 8.4 Hz, Py-*H*), 7.74 (dt, 1H, *J* = 4.0, 7.2 Hz, Py-*H*), 7.59 (dt, 1H, *J* = 4.0, 7.2 Hz, Py-*H*), 7.50 (t, 1H, *J* = 8.0 Hz, Py-*H*), 7.25 (dt, 2H, *J* = 4.0, 7.2 Hz, Ph-*H*, Py-*H*), 6.86 (d, 1H, *J* = 8.0 Hz, Ph-*H*), 6.58 (d, 1H, *J* = 8.4 Hz, Ph-*H*), 6.43 (d, 1H, *J* = 7.2 Hz, Ph-*H*), 6.18 (s, 2H, CH<sub>2</sub>), 3.66 (s, 3H, OCH<sub>3</sub>), 3.60 (s, 3H, OCH<sub>3</sub>); <sup>13</sup>C NMR (DMSO-*d*<sub>6</sub>, 100 MHz, ppm):  $\delta$  = 163.49, 163.12, 155.28, 150.00, 147.84, 142.60, 140.47, 140.25, 137.20, 123.81, 123.08, 119.98, 117.78, 113.46, 111.77, 111.44, 109.34, 53.62, 53.21, 50.00; elemental analysis calcd for 1 [C<sub>20</sub>H<sub>18</sub>Cl<sub>2</sub>N<sub>4</sub>O<sub>2</sub>Zn (482.67)]: C, 49.77; H, 3.76; N, 11.16%; found: C, 49.92; H, 3.63; N, 11.31%.

#### Preparation of {[CdL<sup>1</sup>Cl<sub>2</sub>]}<sub>2</sub> (2)

A mixture of L<sup>1</sup> (34.8 mg, 0.1 mmol) and CdCl<sub>2</sub>·2.5H<sub>2</sub>O (34.7 mg, 0.1 mmol) was dissolved in CH<sub>3</sub>CN (8.0 mL), which was placed in a 10 mL glass flask and heated at 80 °C for 4 days. After the sample was cooled to the room temperature, the mixed solution was filtered and kept for evaporation at room temperature. The yellow crystals appeared after 7 days. Yield: 42.3 mg (40%); UV (CH<sub>3</sub>OH, 25 °C):  $\lambda_{\max}$  (nm) = 238, 279, 318; FT-IR (KBr, cm<sup>-1</sup>):  $\nu$  = 3455 (m), 3286 (m), 3252 (m), 3085 (w,  $\nu_{\text{Py}}$ , C-H), 2924 (w), 2856 (w), 1663 (s), 1593 (s), 1473 (s), 1450 (s), 1386 (s), 1290 (s), 1217 (m), 1174 (m), 1087 (m), 1010 (m), 1027 (m), 795 (m), 733 (m); <sup>1</sup>H NMR (400 MHz, DMSO-*d*<sub>6</sub>, ppm):  $\delta$  = 7.99 (d, 1H, *J* = 7.2 Hz, Py-*H*), 7.90 (d, 1H, *J* = 8.0 Hz, Py-*H*), 7.74 (dt, 1H, *J* = 3.6, 6.4 Hz, Py-*H*), 7.61 (dt, 1H, *J* = 4.0, 7.2 Hz, Py-*H*), 7.27 (m, 4H, *J* = 3.6, 6.8 Hz, Py-*H*, Ph-*H*), 6.93 (d, 1H, *J* = 8.0 Hz, Ph-*H*), 6.62 (d, 1H, *J* = 8.4 Hz, Ph-*H*), 6.43 (d, 1H, *J* = 7.2 Hz, Py-*H*), 6.21 (s, 2H, CH<sub>2</sub>), 3.67 (s, 3H, OCH<sub>3</sub>), 3.61 (s, 3H, OCH<sub>3</sub>); <sup>13</sup>C NMR (DMSO-*d*<sub>6</sub>, 100 MHz, ppm):  $\delta$  = 163.48, 163.15, 155.23,

150.02, 147.64, 142.64, 140.45, 140.13, 137.28, 123.66, 123.18, 119.95, 117.68, 113.47, 111.69, 111.46, 109.64, 53.52, 53.46, 50.24; elemental analysis calcd for 2 [C<sub>20</sub>H<sub>18</sub>Cl<sub>2</sub>N<sub>4</sub>O<sub>2</sub>Cd (529.68)]: C, 45.35; H, 3.43; N, 10.58%; found: C, 45.46; H, 3.28; N, 10.64%.

#### Preparation of [Cd(L<sup>1</sup>)<sub>2</sub>(NO<sub>3</sub>)<sub>2</sub>]·H<sub>2</sub>O (3)

Complex 3 was prepared using a similar procedure to that described for complex 2, except using Cd(NO<sub>3</sub>)<sub>2</sub>·4H<sub>2</sub>O (30.8 mg, 0.1 mmol) instead of CdCl<sub>2</sub>·2.5H<sub>2</sub>O and L<sup>1</sup> (69.6 mg, 0.2 mmol) instead of L<sup>1</sup> (34.8 mg, 0.1 mmol). After the sample was cooled to room temperature, the mixed solution was filtered and kept for evaporation at room temperature. The yellow crystals appeared after 7 days. Yield: 28.4 mg (30%); UV (CH<sub>3</sub>OH, 25 °C):  $\lambda_{\max}$  (nm) = 222, 295, 337; FT-IR (KBr, cm<sup>-1</sup>):  $\nu$  = 3478 (m), 3084 (w,  $\nu_{\text{Py}}$ , C-H), 2989 (w), 2950 (w), 2856 (w), 1596 (s), 1579 (s), 1501 (s), 1471 (s), 1428(s), 1382 (s), 1304 (s), 1060 (m), 1025 (m), 807 (m), 750 (m), 563 (m), 433 (m); <sup>1</sup>H NMR (DMSO-*d*<sub>6</sub>, 400 MHz, ppm):  $\delta$  = 8.02 (d, 1H, Py-*H*), 7.87 (d, 1H, Py-*H*), 7.76 (d, 1H, Py-*H*), 7.63 (m, 1H, Py-*H*), 7.52 (m, 1H, Ph-*H*), 7.29 (m, 2H, CH<sub>2</sub>), 6.89 (d, 1H, Ph-*H*), 6.63 (t, 1H, Py-*H*), 6.43 (d, 1H, Py-*H*), 6.22 (d, 2H, Ph-*H*), 3.68 (s, 3H, OCH<sub>3</sub>), 3.62 (s, 3H, OCH<sub>3</sub>); <sup>13</sup>C NMR (DMSO-*d*<sub>6</sub>, 100 MHz, ppm):  $\delta$  = 162.86, 162.19, 154.21, 149.54, 147.21, 139.82, 136.81, 131.18, 122.22, 119.20, 116.69, 114.53, 112.88, 110.84, 110.54, 108.51, 99.18, 52.86, 52.26, 49.25; elemental analysis calcd for 3 [C<sub>40</sub>H<sub>38</sub>N<sub>10</sub>O<sub>11</sub>Cd (947.21)]: C, 50.72; H, 4.04; N, 14.79%; found: C, 50.65; H, 3.87; N, 14.85%.

#### Preparation of [HgL<sup>1</sup>Cl<sub>2</sub>] (4)

A solution of HgCl<sub>2</sub> (37.2 mg, 0.1 mmol) in CH<sub>3</sub>OH (5 mL) was added to a solution of L<sup>1</sup> (34.8 mg, 0.1 mmol) in CH<sub>2</sub>Cl<sub>2</sub> (25 mL). The mixture was stirred under reflux for 8 hours. After cooling to room temperature, the resulting solution was removed by filtration. The filtrate was kept for evaporation at room temperature for 3 days. Crystals suitable for X-ray structure determination were picked from the solution. Yield: 42.3 mg (60%); UV (CH<sub>3</sub>OH, 25 °C):  $\lambda_{\max}$  (nm) = 237, 279, 319; FT-IR (KBr, cm<sup>-1</sup>):  $\nu$  = 3444 (m), 3082 (w,  $\nu_{\text{Py}}$ , C-H), 2989 (w), 2950 (w), 1604 (s), 1575 (s), 1470 (s), 1414 (s), 1350 (s), 1312 (s), 1264 (m), 1151 (m), 1022 (m), 820 (m), 755 (m), 439 (w); <sup>1</sup>H NMR (DMSO-*d*<sub>6</sub>, 400 MHz, ppm):  $\delta$  = 7.98 (d, 1H, *J* = 7.2 Hz, Py-*H*), 7.86 (t, 1H, *J* = 8.4 Hz, Py-*H*), 7.75 (dt, 1H, *J* = 3.6, 6.8 Hz, Py-*H*), 7.59 (dt, 1H, *J* = 3.6, 6.8 Hz, Py-*H*), 7.52 (t, 1H, *J* = 8.0 Hz, Py-*H*), 7.27 (dt, 2H, *J* = 4.0, 7.2 Hz, Py-*H*, Ph-*H*), 6.88 (d, 1H, *J* = 8.4 Hz, Ph-*H*), 6.59 (d, 1H, *J* = 8.0 Hz, Ph-*H*), 6.46 (d, 1H, *J* = 7.2 Hz, Ph-*H*), 6.17 (s, 2H, CH<sub>2</sub>), 3.68 (s, 3H, OCH<sub>3</sub>), 3.59 (s, 3H, OCH<sub>3</sub>); <sup>13</sup>C NMR (DMSO-*d*<sub>6</sub>, 100 MHz, ppm):  $\delta$  = 163.51, 163.19, 155.14, 150.08, 147.59, 142.38, 140.53, 140.28, 137.10, 123.91, 123.19, 119.94, 117.85, 113.57, 111.92, 111.52, 109.41, 53.67, 53.23, 50.01; elemental analysis calcd for 4 [C<sub>20</sub>H<sub>18</sub>Cl<sub>2</sub>N<sub>4</sub>O<sub>2</sub>Hg (617.87)]: C, 38.88; H, 2.94; N, 9.07%; found: C, 38.76; H, 2.78; N, 9.20%.

## Preparation of [ZnL<sup>2</sup>Cl<sub>2</sub>] (5)

A solution of ZnCl<sub>2</sub> (13.6 mg, 0.1 mmol) in CH<sub>3</sub>CN (10 mL) was added to a solution of L<sup>2</sup> (22.4 mg, 0.1 mmol) in CH<sub>3</sub>CN (10 mL). The mixture was stirred under reflux for 8 hours. After cooling to room temperature, the resulting solution was removed by filtration. The filtrate was kept for evaporation at room temperature for 5 days. Crystals suitable for X-ray structure determination were picked from the solution. Yield: 28.8 mg (80%); UV (CH<sub>3</sub>OH, 25 °C): λ<sub>max</sub> (nm) = 231, 271, 313; FT-IR (KBr): ν = 3058 (w, ν<sub>Py</sub>, C-H), 2948 (w), 2858 (w), 1586 (s), 1469 (s), 1451 (s), 1317 (m), 1267 (m), 1069 (m), 1021 (m), 903 (m), 752 (s), 434 (m) cm<sup>-1</sup>; <sup>1</sup>H NMR (400 MHz, DMSO-*d*<sub>6</sub>, 25 °C): δ = 13.11 (s, 1H, imidazole-H), 8.18 (d, 1H, *J* = 7.2 Hz, Py-H), 7.96 (d, 1H, *J* = 8.0 Hz, Py-H), 7.90 (t, 1H, *J* = 7.6 Hz, Py-H), 7.65 (m, 1H, Ph-H), 7.01 (d, 1H, *J* = 8.4 Hz, Ph-H), 6.71 (d, 1H, *J* = 8.4 Hz, Ph-H), 6.52 (d, 1H, *J* = 7.2 Hz, Ph-H), 3.74 (s, 3H, OCH<sub>3</sub>); elemental anal. calcd for 5 [C<sub>13</sub>H<sub>11</sub>Cl<sub>2</sub>N<sub>3</sub>OZn (361.54)]: C 43.19; H 3.07; N 11.62%; found: C 43.25; H 3.22; N 11.54%.

## X-ray structure determination

Suitable cubic single-crystals were selected for single-crystal X-ray diffraction analysis. The data were collected on a Bruker Apex II CCD diffractometer using graphite-monochromated Mo-Kα radiation (λ = 0.71073 Å) at 293 ± 2 K. Data processing was accomplished with the SAINT processing program. The structures were solved by direct methods and refined by full-matrix, least squares based on *F*<sup>2</sup> using the SHELXTL 5.1 software package.<sup>11</sup> The IIB group metal atoms were first located, and then the oxygen, carbon, nitrogen, chlorine and

hydrogen atoms in L<sup>1</sup> and complexes 1–5 were found in Fourier difference maps. All non-hydrogen atoms were refined anisotropic thermal parameters. Crystallographic data and structural refinements for L<sup>1</sup> and 1–5 are summarized in Table 1. CCDC reference numbers: 938861 for L<sup>1</sup>, 938858 for 1, 938859 for 2, 933809 for 3, 938860 for 4, and 946739 for 5.

## Results and discussion

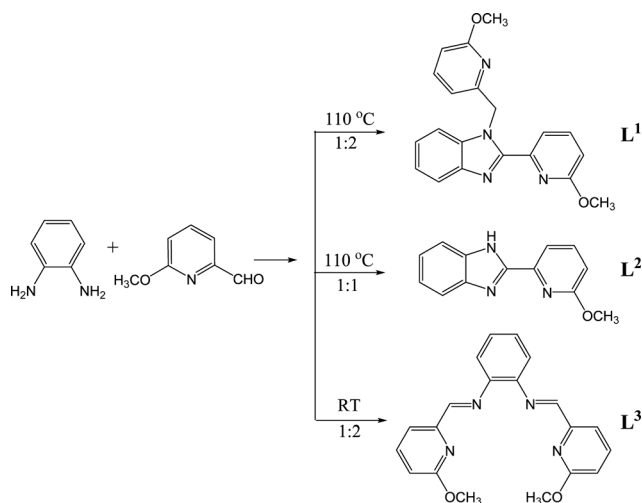
### Synthesis and characterization

The synthetic route to the ligand is shown in Scheme 1. Benzimidazole derivatives L<sup>1</sup> and L<sup>2</sup> were synthesized according to modified methods.<sup>12</sup> As shown in Scheme 2, the salen-type ligand L<sup>3</sup> was obtained by condensation of 1,2-diaminobenzene and 6-methoxy-2-pyridinecarboxaldehyde in a 1:2 molar ratio at room temperature. L<sup>3</sup> could convert into the benzimidazole derivative L<sup>1</sup> in refluxing toluene in reasonable yield. This type of transformation is well known and in the case of L<sup>1</sup> produces two 2-methoxy-pyridyl substituents. Analogously, treatment of 1,2-diaminobenzene with 6-methoxy-2-pyridinecarboxaldehyde in 1:1 molar ratio in toluene at ambient temperature produces the yellow Schiff-base. Furthermore, the mono-imine Schiff-base precursor is converted into the off-white L<sup>2</sup> in refluxing toluene. In addition, if this reaction is carried out in low boiling point solvents, such as CH<sub>3</sub>OH, C<sub>2</sub>H<sub>5</sub>OH, CH<sub>3</sub>CN, and THF, the yields of L<sup>1</sup> and L<sup>2</sup> are very low. Therefore, temperature plays a subtle role in synthesis. The preparation of 1–5 includes two methods: for 1, 4 and 5, the typical reaction of zinc(II)/mercury(II) chloride with ligand is carried out under refluxing conditions; for 2 and 3, the reaction of cadmium salts with L<sup>1</sup> is carried out under

**Table 1** Crystal data and structure parameters for ligand L<sup>1</sup> and complexes 1–5

	L <sup>1</sup>	1	2	3	4	5
Empirical formula	C <sub>20</sub> H <sub>18</sub> N <sub>4</sub> O <sub>2</sub>	ZnC <sub>20</sub> H <sub>18</sub> Cl <sub>2</sub> N <sub>4</sub> O <sub>2</sub>	CdC <sub>20</sub> H <sub>18</sub> Cl <sub>2</sub> N <sub>4</sub> O <sub>2</sub>	CdC <sub>40</sub> H <sub>38</sub> N <sub>10</sub> O <sub>11</sub>	HgC <sub>20</sub> H <sub>18</sub> Cl <sub>2</sub> N <sub>4</sub> O <sub>2</sub>	C <sub>13</sub> H <sub>11</sub> Cl <sub>2</sub> ON <sub>3</sub> Zn
Formula weight	346.38	482.67	529.68	947.21	617.87	361.54
Crystal system	Monoclinic	Monoclinic	Monoclinic	Monoclinic	Triclinic	Triclinic
Space group	<i>P</i> 2 <sub>1</sub> / <i>c</i>	<i>P</i> 2 <sub>1</sub> / <i>n</i>	<i>P</i> 2 <sub>1</sub> / <i>n</i>	<i>P</i> 2 <sub>1</sub> / <i>c</i>	<i>P</i> $\bar{1}$	<i>P</i> $\bar{1}$
<i>a</i> (Å)	11.532(2)	15.010(3)	10.023(2)	11.048(2)	7.995(16)	7.346(15)
<i>b</i> (Å)	13.619(3)	9.253(19)	14.669(3)	18.326(5)	11.283(2)	9.400(19)
<i>c</i> (Å)	11.371(2)	16.741(3)	14.429(3)	19.723(5)	11.996(2)	10.700(2)
α (°)	90	90	90	90	97.51(3)	101.75(3)
β (°)	95.74(3)	113.64(3)	96.56(3)	91.20(2)	103.89(3)	90.16(3)
γ (°)	90	90	90	90	102.50(3)	92.82(3)
<i>V</i> (Å <sup>3</sup> )	1776.9(6)	2130.0(7)	2107.6(7)	3992.3(17)	1006.3(3)	722.4(3)
<i>Z</i>	4	4	4	4	2	2
<i>T</i> (K)	293(2)	293(2)	293(2)	293(2)	293(2)	293(2)
λ (Å)	0.71073	0.71073	0.71073	0.71073	0.71073	0.71073
ρ <sub>calcd</sub> (g cm <sup>-3</sup> )	1.295	1.505	1.669	1.549	2.039	1.653
μ (mm <sup>-1</sup> )	0.087	1.427	1.313	0.620	7.938	2.066
<i>F</i> (000)	728	984	1056	1904	592	360
θ range (°)	3.04 to 27.48	3.09 to 27.48	3.12 to 27.47	3.01 to 29.22	3.18 to 27.48	3.23 to 27.47
GOF on <i>F</i> <sup>2</sup>	1.034	1.070	1.153	1.028	0.879	0.986
<i>R</i> <sub>1</sub> , w <i>R</i> <sub>2</sub> ( <i>I</i> > 2σ( <i>I</i> )) <sup>a</sup>	<i>R</i> <sub>1</sub> = 0.0435 w <i>R</i> <sub>2</sub> = 0.1106	<i>R</i> <sub>1</sub> = 0.0411 w <i>R</i> <sub>2</sub> = 0.0895	<i>R</i> <sub>1</sub> = 0.0291 w <i>R</i> <sub>2</sub> = 0.0834	<i>R</i> <sub>1</sub> = 0.0414 w <i>R</i> <sub>2</sub> = 0.0939	<i>R</i> <sub>1</sub> = 0.0337 w <i>R</i> <sub>2</sub> = 0.0894	<i>R</i> <sub>1</sub> = 0.0785 w <i>R</i> <sub>2</sub> = 0.2118
<i>R</i> <sub>1</sub> , w <i>R</i> <sub>2</sub> (all data) <sup>a</sup>	<i>R</i> <sub>1</sub> = 0.0739 w <i>R</i> <sub>2</sub> = 0.1229	<i>R</i> <sub>1</sub> = 0.0649 w <i>R</i> <sub>2</sub> = 0.0839	<i>R</i> <sub>1</sub> = 0.0350 w <i>R</i> <sub>2</sub> = 0.0866	<i>R</i> <sub>1</sub> = 0.0650 w <i>R</i> <sub>2</sub> = 0.1103	<i>R</i> <sub>1</sub> = 0.0387 w <i>R</i> <sub>2</sub> = 0.0963	<i>R</i> <sub>1</sub> = 0.1369 w <i>R</i> <sub>2</sub> = 0.3374

$$^a R_1 = \sum ||F_o| - |F_c|| / \sum |F_o|; wR_2 = [\sum [w(F_o^2 - F_c^2)^2] / \sum [w(F_o^2)^2]]^{1/2}.$$



Scheme 1 The synthetic procedure for ligands  $L^1$ – $L^3$ .

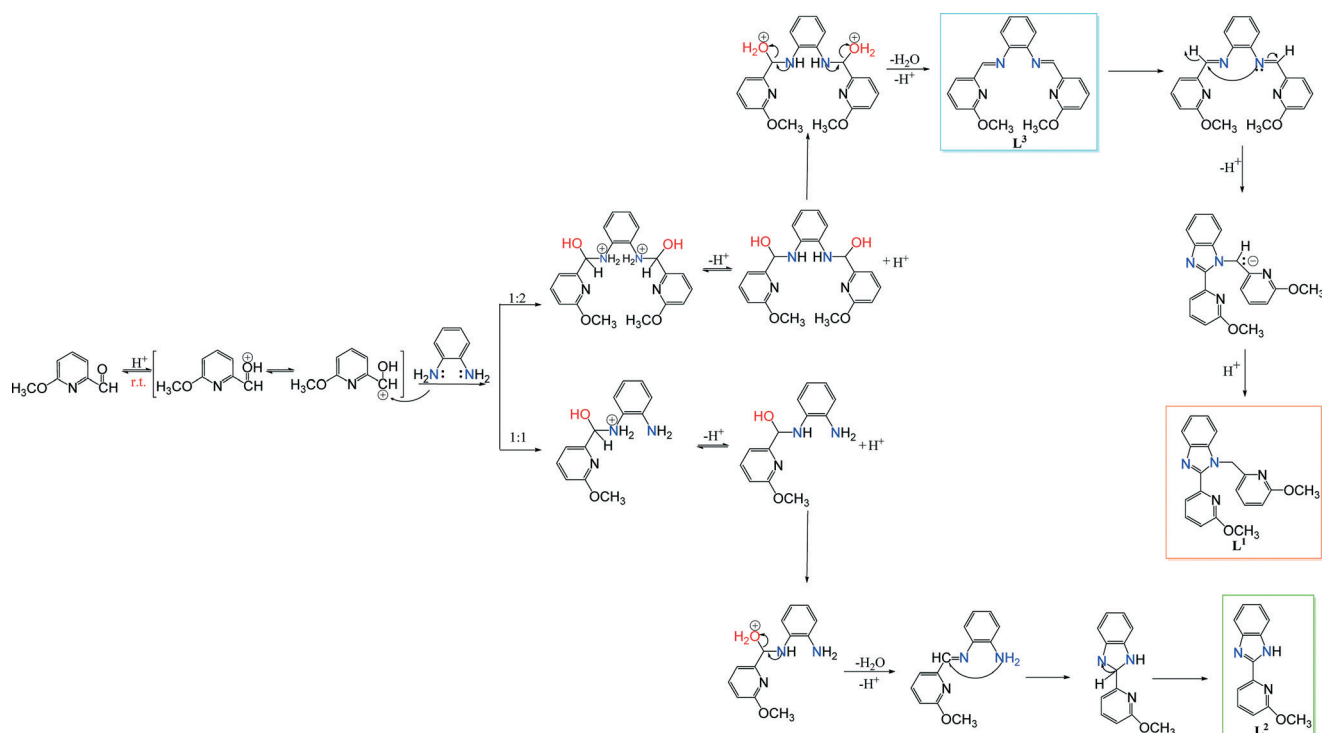
solvothermal conditions. Crystals of  $L^1$  and 1–5 suitable for X-ray diffraction studies were obtained by evaporating the recrystallized solution and the resulting solutions of corresponding complexes, respectively. 1–5 are stable in solution and in the solid state upon extended exposure to air. This remarkable stability is attributable to the bidentate chelation of the ligand to the metal center. Ligands have good solubility in common organic solvents; 1–5 are slightly soluble in low polarity solvents such as *n*-hexane, toluene and benzene, and soluble in medium and high polarity solvents.

In the FT-IR spectra (Fig. S1, ESI<sup>†</sup>), the characteristic vibrations of 2-substituted pyridines are shifted to higher

frequency and are split, from 1316, 1031, 989 and 747  $\text{cm}^{-1}$  for  $L^1$  (1308, 1024, 989 and 750  $\text{cm}^{-1}$  for  $L^2$ ) to 1322, 1052, 1024 and 755  $\text{cm}^{-1}$  for 1 (1350, 1087, 1010 and 768  $\text{cm}^{-1}$  for 2; 1382, 1060, 1025 and 750  $\text{cm}^{-1}$  for 3; 1350, 1079, 1022 and 755  $\text{cm}^{-1}$  for 4; 1317, 1029, 1023 and 764  $\text{cm}^{-1}$  for 5). This is indicative of the coordination of the ligand through the imidazolic and pyridinic nitrogen atoms. For 3, a broad band at 3472  $\text{cm}^{-1}$  indicates the presence of crystallisation water molecules. A strong band at *ca.* 1600  $\text{cm}^{-1}$  is assignable to the pyridine-ring vibrations. Extensive studies have shown that four bands of 3 near 1480 ( $\nu_1$ ), 1304 ( $\nu_4$ ), 1025 ( $\nu_2$ ) and 806 ( $\nu_3$ )  $\text{cm}^{-1}$  can be assigned to vibrations of the coordinated nitrate group.<sup>13</sup> The difference between the  $\nu_4$  and the  $\nu_1$  peak positions is approximately 190  $\text{cm}^{-1}$ , which is typical for  $\eta^2$ -chelation of the nitrate groups.<sup>14</sup> The much smaller splitting of in-plane bending  $\text{NO}_3$  vibrations (at 766 and 750  $\text{cm}^{-1}$ , 16  $\text{cm}^{-1}$ ) indicates the presence of a monodentate nitrate group.<sup>15</sup> Coordination of the nitrogen atoms to the IIB group metal center from the benzimidazole and pyridine groups is substantiated by the far-infrared band (430  $\text{cm}^{-1}$ ) corresponding to  $\nu(\text{M-N})$  vibrational mode.

### Description of crystal structures

The novel bis-methoxy pyridyl substituted benzimidazole  $L^1$  belongs to the centric monoclinic space group  $P2_1/c$ . Both pyridyl groups are twisted with respect to the planar benzimidazole unit in order to reduce the steric interactions (Fig. 1). The two pyridine rings are virtually perpendicular to each other (dihedral angle 87.81°), and the dihedral angles



Scheme 2 The mechanism of the formation of  $L^1$ – $L^3$ .

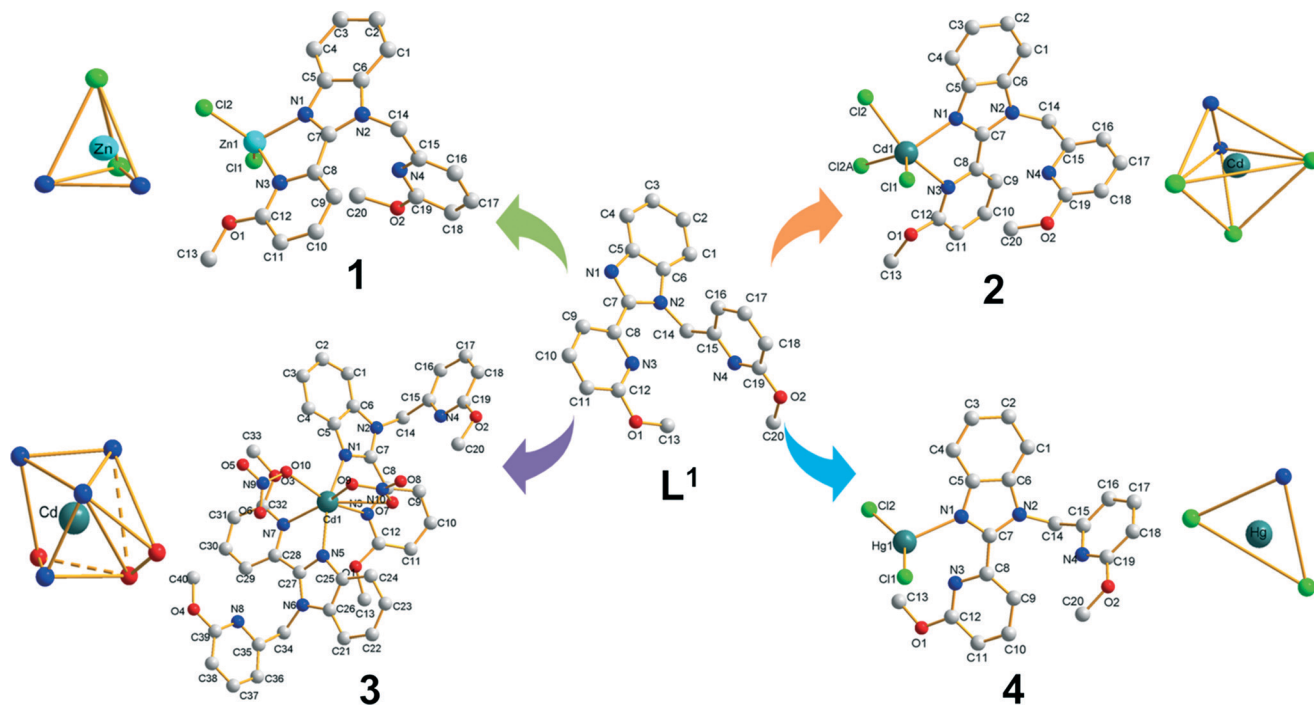


Fig. 1 Molecular structures of ligand  $L^1$  and complexes 1–4, the water molecule in 3 is omitted for clarity. The coordination sphere of the  $M^{2+}$  centre displays tetrahedron (1), trigonal bipyramid (2), distorted monocapped trigonal prism (3) and triangle geometries (4), respectively.

between the planar benzimidazole and each pyridine ring are  $2.49^\circ$  and  $85.87^\circ$ , respectively.

Complex 1 belongs to the centric monoclinic space group  $P2_1/n$ . The zinc(II) atom is four coordinated, and bonded to two nitrogen atoms derived from the  $N^{\wedge}N$  ligand and two chlorine atoms, forming a tetrahedral geometry. The dihedral angle between the benzimidazolyl ring and pyridyl ring linked by a C–C single bond is  $3.34^\circ$ . Compared to  $L^1$ , the dihedral angle between the other pyridyl ring and the benzimidazolyl ring ( $76.96^\circ$ ) decreases upon coordination. The Zn–N (pyridine) bond length [ $2.097(3)$  Å] is longer than the Zn–N (imidazole) bond length [ $2.031(3)$  Å]. The average Zn–N distance of  $2.064$  Å is close to the values found in other Zn(II) complexes.<sup>16</sup> The two chlorine atoms (Cl1 and Cl2) are located above and below the planar benzimidazole and zinc atom. The distances between benzimidazole and the two coordinated chlorine anions are  $1.917(2)$  Å and  $1.881(1)$  Å, respectively.

Complex 2 is a dimer structure in which the  $Cd^{2+}$  cation takes a five-coordinated geometry with a typical trigonal bipyramid (Fig. 1). In the asymmetric structural units, each Cd(II) center is bidentately chelated by  $N^{\wedge}N$   $L^1$  via two nitrogen atoms (N1 and N2), and the remaining sites are occupied by three chlorine atoms (fully occupied Cl1, half-occupied Cl2). Examination of the dihedral angle between the two pyridine groups reveals the angle is approximately perpendicular ( $89.37^\circ$ ). Closer inspection reveals the dihedral angles to planar benzimidazole are  $21.35^\circ$  and  $71.69^\circ$ , respectively. The changes of dihedral angles are compressed compared to the free  $L^1$  in order to accommodate metal ions. It

gives rise to a five-membered ring (Cd1–N1–C8–C7–N3) after coordination. The dihedral angle between the five-membered ring and the benzimidazole group is  $6.77^\circ$ . Simultaneously, the appearance of five-membered ring system enhances the stability of the structure. The Cd–N (imidazole) bond length [ $2.286(2)$  Å] is significantly shorter than the Cd–N (pyridyl) bond length [ $2.393(2)$  Å], which is consistent with the structural data reported previously.<sup>17</sup> The N–Cd–N bond angle is  $70.55(4)^\circ$ , which is much smaller than the ideal bond angle of an  $sp^3$  hybrid orbital ( $109.28^\circ$ ). The neighboring molecules are connected through two bridging Cl2 and Cl2A atoms to construct a dimer structure (Fig. S5, ESI<sup>†</sup>). There is no intermolecular packing in 2. However, the structure of 2 is stabilized by hydrogen bonds between the Cl2 atom and C4 atom of the adjacent units (Fig. S5, ESI<sup>†</sup>). The distance of  $Cl\cdots C$  is  $3.541$  Å, and the bond angle of  $Cl\cdots H-C$  is  $141.93^\circ$ , which are similar to results from the literature reported previously.<sup>18</sup>

The asymmetric unit of 3 contains an independent  $Cd^{2+}$  cation, two benzimidazole ligands, two nitrate anions and a solvated water molecule (Fig. 1). The Cd(II) center is coordinated to four nitrogen atoms from two  $L^1$ , and three oxygen atoms from monodentate and bidentate nitrate anions. The 7-coordinated geometry around  $Cd^{2+}$  cation is a distorted monocapped trigonal prism, with Cd–N and Cd–O distances in the range of  $2.279(2)$ – $2.532(3)$  Å and  $2.374(3)$ – $2.801(2)$  Å. The Cd-bridging angles of N1–Cd–N3, N5–Cd–N7 and O5–Cd–O7 are  $68.64(8)$ ,  $71.38(9)$  and  $48.12(3)$ , respectively. The Cd–N distance to the benzimidazole ring is slightly shorter than that to the pyridyl donor, as was observed recently for an

analog.<sup>17</sup> The adjacent pyridyl groups and benzimidazole plane are twisted by dihedral angles of 16.45° and 28.30°, respectively. Two benzimidazole ligands exhibit the cross style, whose dihedral angle is 71.45°. Intriguingly, the adjacent pyridyl group in one **L**<sup>1</sup> is parallel-like with a methylene group bridging the pyridyl group on the other **L**<sup>1</sup>, the corresponding angles are 21.08° and 26.09°, respectively. The structure of **3** is also stabilized by the hydrogen bonds between the O1W atom and O5 atom of the adjacent units (Fig. S6, ESI†). The distance of O···O is 3.015 Å, and the bond angle of O···H–O is 146.58°, which are similar to results from the literature reported previously.<sup>19</sup>

Akin to complex **1**, complex **4** belongs to the centric triclinic space group  $P\bar{1}$ . The Hg<sup>II</sup> center is linked through only one nitrogen atom of the benzimidazole group and two chlorine atoms (Fig. 1). The nitrogen atom from the pyridyl group could not participate in the coordination. Thus, the three-coordinated Hg(II) atom forms a planar triangle. As aforementioned, although the complexes **1**–**4** use the same ligand, the reason for the rare three-coordinated system has two contexts as follows: (1) the ionic radius clearly plays a role in directing the architecture of the resulting complex. The ionic radius of Hg(II) is bigger compared with that of Zn/Cd(II), which decreases the electrostatic attraction between ligand and metal atom. The intensity of the bond also weakens along with the increase of ionic radius. (2) The steric hindrance of ligand can influence the forming of bonds around the metal ion. In order to eliminate repulsive forces, an optimized configuration may stabilize the structure of complex. Inspection of the parameters of **4** reveals the Hg–N1 bond distance is 2.318(3) Å and 2.845(4) Å for the distance between Hg(II) and un-coordinated N3 atom. Similar to complexes **2** and **3**, a three-dimensional supramolecular network formed through C–H···Cl hydrogen bonded interactions (Fig. S7, ESI†).

Complex **5** belongs to the centric triclinic space group  $P\bar{1}$ . In analogy to **1**, the centre metal Zn<sup>2+</sup> ion is four coordinate with a typical tetrahedron geometry (Fig. 2a). Each zinc center is bidentately chelated by N<sup>N</sup> **L**<sup>2</sup> *via* two nitrogen atoms (N1 and N2), and the remaining sites are occupied by two chlorine atoms (Cl1 and Cl2). The dihedral angle between the pyridyl group and benzimidazole is approximate parallel (1.69°). The Zn–N (imidazolyl) bond [2.054(2) Å] is significantly shorter than the Zn–N (pyridyl) bond [2.116(2) Å], which is consistent with the structural data reported previously.<sup>16</sup> The N–Zn–N bond angle is 79.60(4)°, which is much smaller than the ideal bond angle of an sp<sup>3</sup> hybrid orbital (109.28°). However, intermolecular Cl···H–N hydrogen bonding interactions are present within each layer and further linked to construct a 1D chain structure along the [010] direction (Fig. 2b). The distances of Cl1···N3 and Cl2···N3 are 3.234 and 3.431 Å, respectively. The bond angles of Cl1···H3–N3 and Cl2···H3–N3 are 124.53° and 145.36°, respectively. There are weak  $\pi$ – $\pi$  stacking interactions between benzimidazole ring and pyridine ring [the distance is 3.702(2) Å] in the crystal lattices of **5** (Fig. 2c) that help to create self-assembled supramolecular frameworks. For **1**–**5**, although **L**<sup>1</sup> has a richly coordinated

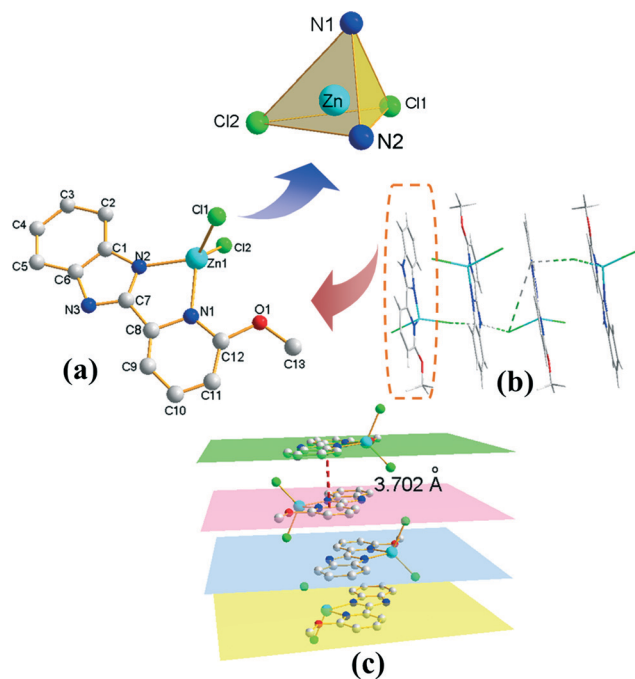


Fig. 2 (a) Molecular structure of complex **5**, all hydrogen atoms are omitted for clarity. (b) The stick view of a 1D chain generated by the hydrogen bonds Cl···H–N in **5** along the [100] direction. (c) View of the  $\pi$ – $\pi$  stacking interactions in **5**.

site, it plays the role of a neutral bidentate chelator. Two oxygen atoms from different –OCH<sub>3</sub> groups do not coordinate to the metal center due to the high nitrophilicity of the transition metals.

### Photophysical properties

The electronic absorption spectra of **L** and **1**–**5** were studied in methanol solution (Fig. 3) and show similar ligand-centered bands in the region of 220–340 nm ( $\epsilon = 6328$ – $38\,581\text{ M}^{-1}\text{ cm}^{-1}$ ). The numerical values of the maximum absorption wavelength and molar extinction coefficients ( $\epsilon$ ) are listed in Table 2. The absorption bands with  $\lambda_{\text{max}} \approx 235$ , 280 and 320 nm were

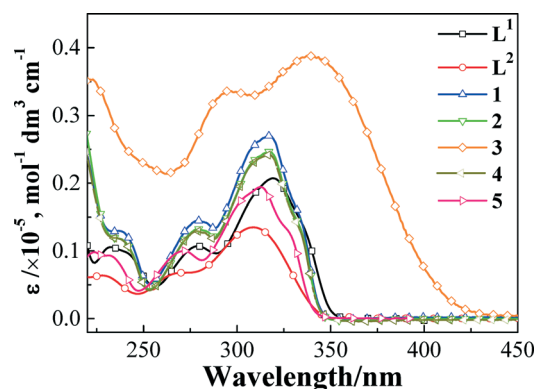


Fig. 3 UV-vis absorption spectra of **L**<sup>1</sup>, **L**<sup>2</sup> and complexes **1**–**5** in CH<sub>3</sub>OH.

Table 2 Photoluminescent data for ligands L<sup>1</sup>, L<sup>2</sup> and complexes 1–5

Complex	Absorption <sup>a</sup> ( $\epsilon$ ) (nm, dm <sup>3</sup> mol <sup>-1</sup> cm <sup>-1</sup> )	Emission ( $\lambda_{\max}$ , nm)	FWHM (nm)	Decay lifetime ( $\tau$ , $\mu$ s)	Quantum yields <sup>a</sup> ( $\Phi$ )	Medium (T/K)	CIE (x, y)		
L <sup>1</sup>	232 (10 522), 279 (10 864), 317 (20 662)	399	31.8	8.87	0.23	CH <sub>3</sub> OH (298)	0.16, 0.08		
		405	61.6	5.12		Solid (298)	0.21, 0.21		
		419 471 <sup>sh</sup>	58.8	10.14		CH <sub>3</sub> OH (77)	0.16, 0.11		
		412 440 <sup>sh</sup> 469 <sup>sh</sup> 497 <sup>sh</sup>	59.7	7.99		Solid (77)	0.23, 0.24		
		470	71.2	5.24		CH <sub>3</sub> OH (298)	0.13, 0.32		
L <sup>2</sup>	228 (6328), 268 (6658), 307 (13 523)	452	59.6	6.01	0.20	CH <sub>2</sub> Cl <sub>2</sub> (298)	0.22, 0.22		
		480	60.5	8.56		Solid (298)	0.14, 0.31		
		474	35.1	6.93		CH <sub>3</sub> OH (77)	0.13, 0.25		
		455	74.8	7.57		CH <sub>2</sub> Cl <sub>2</sub> (77)	0.16, 0.17		
		499	55.2	19.77		Solid (77)	0.19, 0.35		
		406	54.9	9.52		CH <sub>3</sub> OH (298)	0.16, 0.05		
		422	63.0	5.80		Solid (298)	0.18, 0.13		
1	239 (12 822), 279 (14 403), 318 (26 940)	407 497 <sup>sh</sup>	48.0	9.76	0.38	CH <sub>3</sub> OH (77)	0.18, 0.15		
		426 471 <sup>sh</sup> 496 <sup>sh</sup> 516 <sup>sh</sup>	45.1	9.77		Solid (77)	0.18, 0.13		
		402	42.5	8.77		CH <sub>3</sub> OH (298)	0.16, 0.05		
		421	61.6	6.28		Solid (298)	0.17, 0.11		
		408 478 <sup>sh</sup>	48.0	8.79		CH <sub>3</sub> OH (77)	0.17, 0.12		
2	238 (11 549), 279 (11 549), 318 (24 541)	419 443 <sup>sh</sup> 472 <sup>sh</sup> 495 <sup>sh</sup>	53.0	10.74	0.32	Solid (77)	0.20, 0.16		
		402	40.2	10.27		CH <sub>3</sub> OH (298)	0.16, 0.03		
		415	66.0	5.64		Solid (298)	0.21, 0.19		
		399 499 <sup>sh</sup>	36.3	10.74		CH <sub>3</sub> OH (77)	0.19, 0.18		
		412 440 <sup>sh</sup> 496 <sup>sh</sup> 497 <sup>sh</sup>	60.0	7.83		Solid (77)	0.24, 0.24		
3	222 (35 537), 295 (33 673), 337 (38 581)	400	29.4	5.97	0.40	CH <sub>3</sub> OH (298)	0.16, 0.02		
		411	63.5	8.33		Solid (298)	0.21, 0.19		
		402 505 <sup>sh</sup>	26.3	9.84		CH <sub>3</sub> OH (77)	0.20, 0.22		
		406 486 <sup>sh</sup> 529 <sup>sh</sup> 566 <sup>sh</sup> 615 <sup>sh</sup>	159.6	8.33		Solid (77)	0.26, 0.30		
		426	72.6	5.73		CH <sub>3</sub> OH (298)	0.16, 0.07		
4	237 (11 720), 279 (12 805), 319 (24 047)	418	55.3	6.86	0.33	CH <sub>2</sub> Cl <sub>2</sub> (298)	0.18, 0.10		
		434	64.4	9.43		solid (298)	0.19, 0.11		
		427	32.7	7.68		CH <sub>3</sub> OH (77)	0.18, 0.08		
		420	85.5	10.07		CH <sub>2</sub> Cl <sub>2</sub> (77)	0.20, 0.22		
		449	57.5	21.29		solid (77)	0.17, 0.12		
		231 (9381), 271 (9890), 313 (19 399)	426	72.6		5.73	0.26	CH <sub>3</sub> OH (298)	0.16, 0.07
		418	55.3	6.86		CH <sub>2</sub> Cl <sub>2</sub> (298)		0.18, 0.10	
		434	64.4	9.43		solid (298)		0.19, 0.11	
427	32.7	7.68	CH <sub>3</sub> OH (77)	0.18, 0.08					

<sup>a</sup> Recorded in methanol at 298 K, concentration = 10<sup>-5</sup> mol L<sup>-1</sup>. sh = shoulder.

observed for all the ligands and complexes. The bands in the wavelength range 232–239 nm could be assigned to the  $\pi \rightarrow \pi^*$  transition of the benzimidazolyl system. The bands at ca. 280 nm were attributed to the  $\pi \rightarrow \pi^*$  transition centered on C=N groups of the benzimidazolyl units. The bands ca. at 320 nm belong to the  $n \rightarrow \pi^*$  transition of the benzimidazolyl units. Moreover, the low energy absorption bands of 3 (295 nm and 337 nm) are bathochromically shifted as compared with those of the free L<sup>1</sup> (279 nm and 317 nm).<sup>20</sup> Clearly, the  $\epsilon$  value is linearly dependent on the number of 2-(2'-pyridyl)-benzimidazolyl units (one ligand: 1, 2, 4 and 5; two ligands: 3). It is reasonable to infer that the addition of a carrier-transporting group (6-methoxy-2-pyridylmethyl) is useful to enhance the electronic absorption of benzimidazolyl complexes.

The emission spectra of L and 1–5 were recorded in CH<sub>3</sub>OH solution and in the solid state at 298 K and 77 K (Fig. 4). The photophysical data for emission are gathered in Table 2. The process involves light emission that is triggered by crystals that have been previously irradiated with long wavelength UV light (365 nm). The emission is intense and clearly visible. In polar protic solvent CH<sub>3</sub>OH, corresponding

emission peak of L<sup>1</sup> appeared at 399 nm. In comparison with L<sup>1</sup>, complexes 1–4 in CH<sub>3</sub>OH give narrow emission bands (bandwidth at half-height = 29–55 nm) with  $\lambda_{\max}$  = 406, 402, 402 and 400 nm, respectively (Fig. 4). The emission maxima of 1–4 are almost the same as that of the free L<sup>1</sup>, which should be attributed to the  $\pi^* \rightarrow \pi$  transition of ligand. In order to investigate the temperature-dependant emission, cryogenic luminescent behavior measurements were also performed in CH<sub>3</sub>OH. When the excitation and emission spectra are recorded in solution at 77 K, complexes 1–4 display similar maximum emissions at ca. 402–419 nm (Fig. 4c). The distinction between room temperature and cryogenic temperature is the structured bands centered from 471 to 505 nm. In contrast to L<sup>1</sup>, it exhibits hypsochromic shift upon coordination. When the complexes 1–4 and L<sup>1</sup> are examined in the solid state (Fig. 4b and 4d), bathochromic shift from solution to solid is likely to be caused by intermolecular hydrogen bonding interactions existing in the solid form. The hydrogen bonds can effectively decrease the HOMO–LUMO energy gap and influence the ligand-centered  $\pi^* \rightarrow \pi$  transitions.<sup>21</sup> At 77 K, the emissions of solid state at 440–615 nm are more distinctly structured compared to

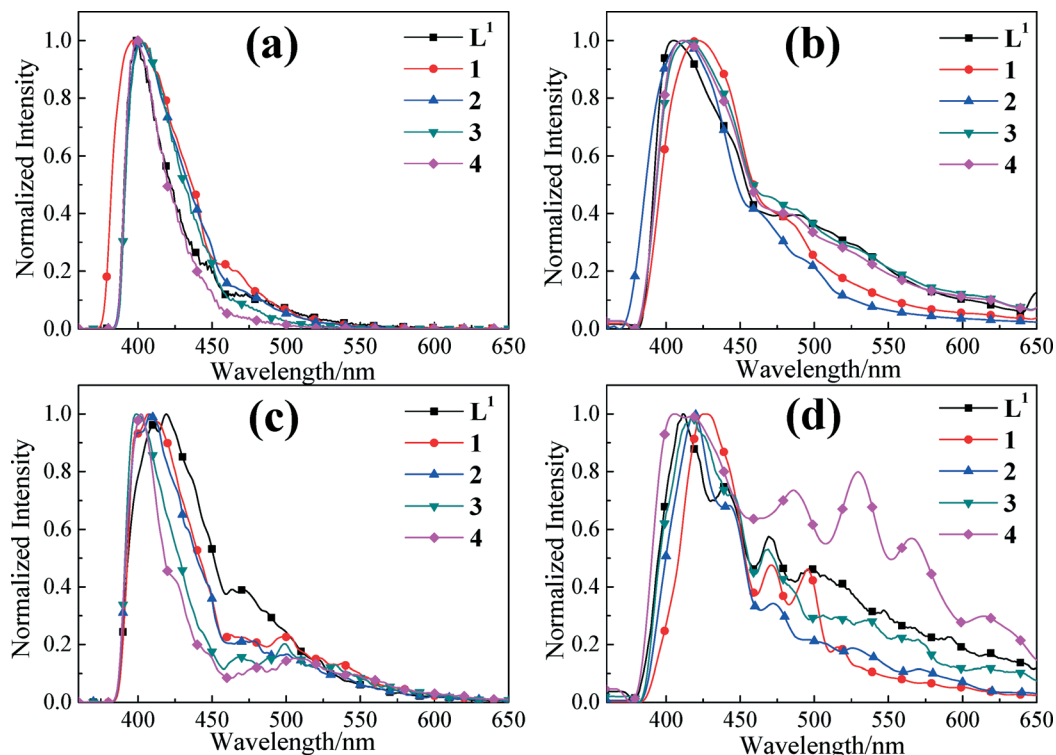


Fig. 4 Emission spectra of  $L^1$  and 1–4 monitored at the longest wavelength of absorption peak (a: 298 K,  $\text{CH}_3\text{OH}$ ; b: 298 K, solid state; c: 77 K,  $\text{CH}_3\text{OH}$ ; d: 77 K, solid state).

those of  $\text{CH}_3\text{OH}$  solution. CIE 1931, which assists the understanding of the color gamut, is also provided. The dominant color gamut of  $L^1$  and complexes 1–4 focuses on blue region according to the calculated values (Fig. 5).

Given the different ligand in 5, we investigated the luminescence of  $L^2$  and 5 both in the solid state and solution at 298 K and 77 K (Fig. 6–7). Solid  $L^2$  and 5 show blue emission. At 298 K, the corresponding emission peak of  $L^2$  in polar

aprotic solvent ( $\text{CH}_2\text{Cl}_2$ ) appeared at 452 nm, emitting sky-blue luminescence. In contrast to  $L^2$ , it is shown that complex 5 displays deep-blue fluorescence emission with the maximum emission at 418 nm. Due to  $\text{ZnCl}_2$  not being luminescent, the luminescence emissions of complex 5 and  $L^2$  both can be attributed to the ligand-centered  $\pi^* \rightarrow \pi$  transitions. With the increase in the polarity (order:  $\text{CH}_2\text{Cl}_2 < \text{CH}_3\text{OH}$ ), the bathochromic shift for 5 occurs from  $\text{CH}_2\text{Cl}_2$  (417 nm) to  $\text{CH}_3\text{OH}$  (425 nm) owing to more polarity in the excited state. A similar emission energy shift is also exhibited in the spectra of  $L^2$  (452 nm in  $\text{CH}_2\text{Cl}_2$  and 470 nm in  $\text{CH}_3\text{OH}$ ). It is ascribed to the donor ability of  $\text{CH}_3\text{OH}$  as a protic solvent. The hydrogen bond donor nature of  $\text{CH}_3\text{OH}$  seems to stabilize the excited state of the electronic transitions through

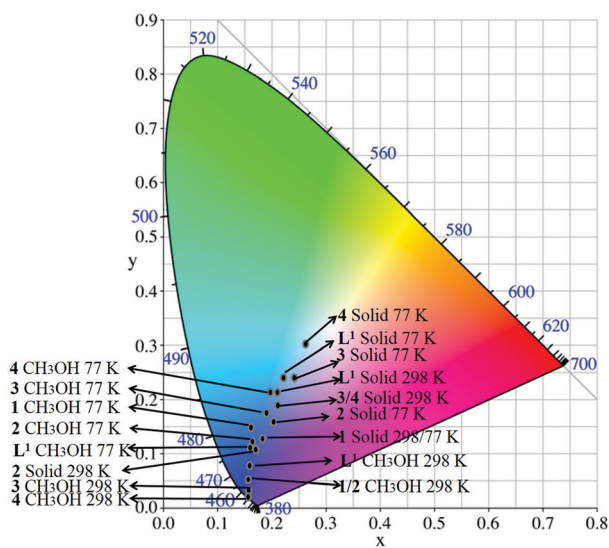


Fig. 5 CIE chromaticity diagram (1931 CIE standard) for ligand  $L^1$  and 1–4.

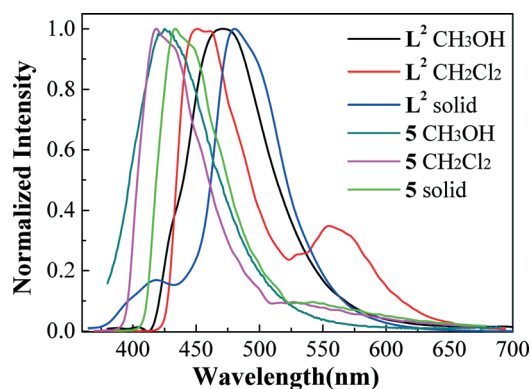


Fig. 6 Normalized emission spectra of  $L^2$  and 5 in  $\text{CH}_3\text{OH}$ ,  $\text{CH}_2\text{Cl}_2$  and in the solid state at 298 K.

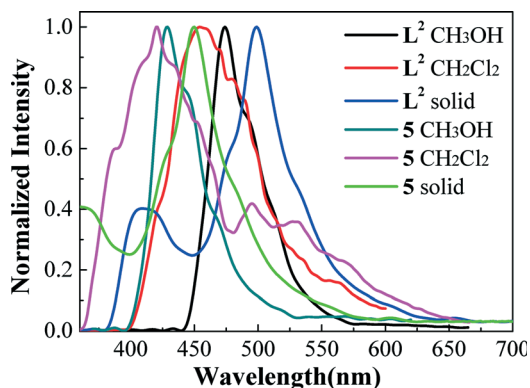


Fig. 7 Normalized emission spectra of  $L^2$  and **5** in  $\text{CH}_3\text{OH}$ ,  $\text{CH}_2\text{Cl}_2$  and in the solid state at 77 K.

solute–solvent interactions and be responsible for the shift of the emission energy.<sup>22</sup> In the solid state, complex **5** and  $L^2$  profiles peak at 432 and 480 nm. Such bathochromic shift relative to that in solution indicates that intermolecular hydrogen bond interactions exist in the solid.<sup>23</sup> The emission spectra in solution at 77 K possessed the similar order compared to those at 298 K. However, the emission maxima in solutions for  $L^2$  and **5** are slightly red-shifted by 3–4 nm as compared to the room temperature values. In the solid state, the emission maxima for  $L^2$  and **5** red-shifted even further (15–19 nm) at 77 K, to  $\lambda_{\text{max}} = 499$  nm ( $L^2$ ) and 449 nm (**5**). We can observe color variations through the CIE coordinates diagram (Fig. 8). The variation from sky-blue of  $L^2$  to deep-blue of **5** undoubtedly implies the coordination of the zinc atom.

The lifetimes of emissions for **L** and **1–5** are in the region of the microsecond scale. The average lifetimes are listed in Table 2. A general trend is that the lifetime of emission at low temperature (77 K) is longer than that at room temperature, which is attributed to the decrease of thermal vibration

and nonradiative transition at low temperature. Meanwhile, the lifetimes of emissions for  $L^1$  and **1–4** in the solid state is shorter than those in solution, which is due to aggregation quenching existing in the solid state.<sup>24</sup> Conversely, the lifetimes of emissions for  $L^2$  and **5** in the solid state are longer than those in solutions, which can be ascribed to the less polar nature of the environment in the solid state.<sup>25</sup> For **5** and  $L^2$ , the lifetimes of emissions in  $\text{CH}_3\text{OH}$  are substantially shortened in comparison with those in  $\text{CH}_2\text{Cl}_2$  under the same test conditions. This phenomenon can be attributed to the following reason: in  $\text{CH}_3\text{OH}$ , a non-radiative process from the intramolecular charge transfer (ICT) state results in a small energy gap between the singlet states and triplet states.<sup>26</sup> To the best of our knowledge, only two other luminescence lifetime measurements of 2-(2-pyridyl)benzimidazole complexes have been previously reported. The first values are in the range of 7.1–8.4  $\mu\text{s}$ , reported by Wang *et al.* in 2005.<sup>27</sup> The second of value is in the range of 0.93 ns, reported by Liang *et al.* in 2009.<sup>28</sup> Obviously, the lifetime of emission for **5** in the solid state (9.43  $\mu\text{s}$  at 298 K, 21.29  $\mu\text{s}$  at 77 K) is longer than that reported above.

The luminescence quantum yield, defined as the ratio of the number of photons emitted to the number of photons absorbed, gives the efficiency of the luminescence process. The quantum yields of  $L^1$ ,  $L^2$  and **1–5** have been determined in  $\text{CH}_3\text{OH}$  solution and were determined to be 0.23, 0.20, 0.38, 0.32, 0.40, 0.33, and 0.26, respectively. As we expected, it was found that the quantum yields of **1–5** are higher than those of the corresponding ligands. In brief, the enhancement after the connection of the ligand to metal center increases the conformational rigidity of the ligands, and hence reduces the non-radioactive deactivation pathways.<sup>29</sup> Meanwhile the quantum yield of the  $\text{Hg(II)}$  complex **4** is lower than that of  $\text{Zn(II)}$  and  $\text{Cd(II)}$  complexes **1–3**. These results

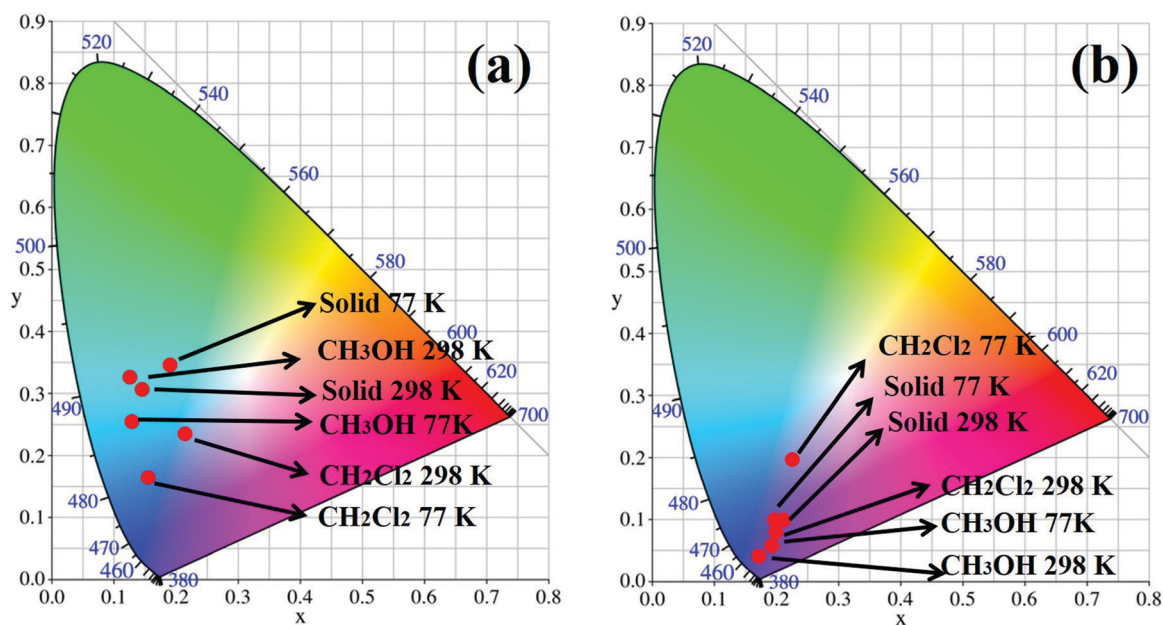


Fig. 8 The corresponding CIE chromaticity diagram of  $L^2$  (a) and **5** (b).

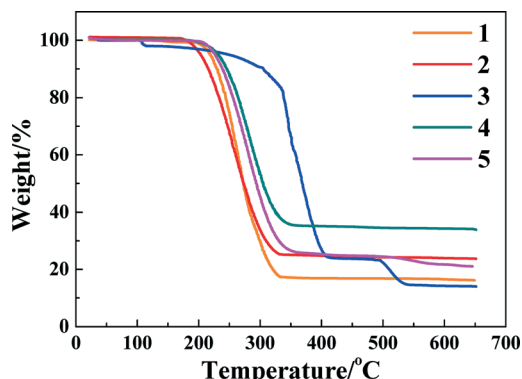


Fig. 9 TG curves of complexes 1–5.

can be easily understood considering the following factor: the Hg(II) cation and the chloride anions can quench the fluorescence and result in luminescence decay.<sup>30</sup> The bulkier configuration of 3 reduces the vibrational motion and avoids the solvents to quench the emission, which is the reason for the higher quantum yield.

### Thermal analysis

Thermogravimetric experiments were conducted to study the thermal stability of complexes 1–5 (Fig. 9), which is an important parameter of inorganic–organic hybrid materials. Complexes 1, 2, 4 and 5 show similar thermal behaviors, which are different from that of 3. The TG curves for 1, 2, 4 and 5 show they are stable up to ca. 215 °C and the organic ligands begin to decompose after this temperature. The TG analysis of 3 shows an initial weight loss of 1.8% in the range 103–112 °C, corresponding to the removal of uncoordinated water molecule (theoretical loss is 1.9%). Upon further heating, the second weight loss of 72.4% in the temperature range of 328–402 °C is attributed to the loss of L<sup>1</sup> (theoretical loss is 73.1%). This step indicates that 3 is stable up to ca. 330 °C, at which temperature it begins to decompose. The third weight loss of 11.1% at 498–532 °C is considered to be the two nitrate anions (theoretical loss is 13.0%). For complexes 1–5, the remaining weight corresponds to the percentage of the M (M = Zn, Cd, Hg) and O components, indicating that the final product is MO.

## Conclusions

The noteworthy feature of our work is success in introducing benzimidazole derivatives ligands L<sup>1</sup> and L<sup>2</sup> into a series of IIB group metal complexes. The formation of complexes proved that the counter anions and ionic radius play a crucial role in the coordination mode of the central metal. The central metal in complexes 1(5), 2 and 4 with Cl<sup>−</sup> counterion are four-, five-, and three-coordinated forming a tetrahedron, trigonal bipyramid and triangle geometries, respectively. The seven-coordinated center metal in 3 ligates two ligands, forming distorted monocapped trigonal prismatic geometry. By using the strategy of modifying, NH is replaced by a pyridine group in order to control the conjugation of the

chelate ligand. The luminescence of the complexes is caused by  $\pi^*-\pi$  electronic transitions centered on the N<sup>−</sup>N chelate ligands. Our investigation shows that two series of IIB group metal complexes with emission colors covering the visible blue region can be achieved.

## Acknowledgements

This work was supported by the National Natural Science Foundation of China (Grant No. 21371040 and 21171044), the National key Basic Research Program of China (973 Program, No. 2013CB632900), the Fundamental Research Funds for the Central Universities (Grant No. HIT. IBRSEM. A. 201409), and the Program for Innovation Research of Science in Harbin Institute of Technology (PIRS of HIT No. A201416 and B201414). Chen wants to thank the support from Academic New Talents Award of Doctoral Post Graduate of Ministry of Education.

## Notes and references

- (a) H. Y. Liu, J. F. Ma, Y. Y. Liu and J. Yang, *CrystEngComm*, 2013, 15, 2699; (b) L. Zhou, Y. Y. Wang, C. H. Zhou, C. J. Wang, Q. Z. Shi and S. M. Peng, *Cryst. Growth Des.*, 2007, 7, 300; (c) M. X. Li, H. Wang, S. W. Liang, M. Shao, X. He, Z. X. Wang and S. R. Zhu, *Cryst. Growth Des.*, 2009, 9, 4626.
- (a) Q. D. Liu, M. S. Mudadu, R. Thummel, Y. Tao and S. Wang, *Adv. Funct. Mater.*, 2005, 15, 143; (b) T. Suzuki, M. Kotera, A. Takayama and M. Kojima, *Polyhedron*, 2009, 28, 2287; (c) Z. Xia, Q. Wei, Q. Yang, C. Qiao, S. Chen, G. Xie, G. Zhang, C. Zhou and S. Gao, *CrystEngComm*, 2013, 15, 86.
- J. G. Malecki, *Polyhedron*, 2010, 29, 2489.
- H. Keypour, R. Azadbakht, S. Salehzadeh, H. A. Rudbari and H. Adams, *Tetrahedron Lett.*, 2009, 50, 169.
- M. Shellaiah, Y. H. Wu, A. Singh, M. V. R. Raju and H. C. Lin, *J. Mater. Chem. A*, 2013, 1, 1310.
- (a) A. Knödler, K. Hübner, T. Sixt and W. Kaim, *Inorg. Chem. Commun.*, 2000, 3, 182; (b) J. Wu, H. Y. Li, L. C. Kang, D. P. Li, Q. L. Xu, Y. C. Zhu, Y. M. Tao, Y. X. Zheng, J. L. Zuo and X. Z. You, *J. Organomet. Chem.*, 2010, 695, 2048.
- (a) X. Yang, R. A. Jones, M. M. Oye, M. Wiester and R. J. Lai, *New J. Chem.*, 2011, 35, 310; (b) X. Ma, X. Li, Y. E. Cha and L. P. Jin, *Cryst. Growth Des.*, 2012, 12, 5227.
- (a) N. C. Desai, A. M. Dodiya and A. H. Makwana, *Med. Chem. Res.*, 2012, 21, 2320; (b) B. Garudachari, M. N. Satyanarayana, B. Thippeswamy, C. K. Shivakumar, K. N. Shivananda, G. Hegde and A. M. Isloor, *Eur. J. Med. Chem.*, 2012, 54, 900; (c) R. V. Patel, P. K. Patel, P. Kumari, D. P. Rajani and K. H. Chikhaliya, *Eur. J. Med. Chem.*, 2012, 54, 41; (d) B. Narasimhan, D. Sharma and P. Kumar, *Med. Chem. Res.*, 2012, 21, 269; (e) B. Roopashree, V. Gayathri, A. Gopi and K. S. Devaraju, *J. Coord. Chem.*, 2012, 65, 4023.
- P. Chen, H. Chen, P. Yan, Y. Wang and G. Li, *CrystEngComm*, 2011, 13, 6237.
- (a) M. Shi, F. Li, T. Yi, D. Zhang, H. Hu and C. Huang, *Inorg. Chem.*, 2005, 44, 8929; (b) S. Viswanathan and A. de Bettencourt-Dias, *Inorg. Chem.*, 2006, 45, 10138.

- 11 Sheldrick, *SHELXL 97 Program for Crystal Structure Refinement*, University of Göttingen, Göttingen, Germany, 1997.
- 12 (a) X. Yang, R. A. Jones, R. J. Lai, A. Waheed, M. M. Oye and A. L. Holmes, *Polyhedron*, 2006, 25, 881; (b) X. Yang, R. A. Jones, M. J. Wiester, M. M. Oye and W.-K. Wong, *Cryst. Growth Des.*, 2007, 10, 970.
- 13 L. Liu, Y. Sun, S. Wei, X. Hu, Y. Zhao and J. Fan, *Spectrochim. Acta, Part A*, 2012, 86, 120.
- 14 (a) P. Yan, W. Sun, G. Li, C. Nei, T. Gao and Z. Yue, *J. Coord. Chem.*, 2007, 60, 1973; (b) W. Wang, Y. Huang and N. Tang, *Spectrochim. Acta, Part A*, 2007, 6, 1058.
- 15 B. Machura, A. Świtlicka, M. Wolff, J. Kusz and R. Kruszynski, *Polyhedron*, 2009, 28, 1348.
- 16 T. Mukherjee, J. C. Pessoa, A. Kumarb and A. R. Sarkar, *Dalton Trans.*, 2012, 41, 5260.
- 17 N. M. Shavaleev, Z. R. Bell, T. L. Easun, R. Rutkaite, L. Swanson and M. D. Ward, *Dalton Trans.*, 2004, 3678.
- 18 R. Fan, Y. Yang, Y. Yin, W. Hasi and Y. Mu, *Inorg. Chem.*, 2009, 48, 6034.
- 19 G. R. Desiraju, *Acc. Chem. Res.*, 1996, 29, 441.
- 20 (a) V. A. Krylova, P. I. Djurovich, M. T. Whited and M. E. Thompson, *Chem. Commun.*, 2010, 46, 6696; (b) Q. Li, P. Yan, P. Chen, G. Hou and G. Li, *J. Inorg. Organomet. Polym.*, 2012, 22, 1174.
- 21 M. Kubinyi, O. Varga, P. Baranyai, M. Kállay, R. Mizsei, G. Tárkányi and T. Vidóczy, *J. Mol. Struct.*, 2011, 1000, 77.
- 22 X. Gong, Y. Y. Ge, M. Fang, Z. G. Gu, S. R. Zheng, W. S. Li, S. J. Hu, S. B. Li and Y. P. Cai, *CrystEngComm*, 2011, 13, 6911.
- 23 Q. Wu, J. A. Lavigne, Y. Tao, M. D'Iorio and S. Wang, *Inorg. Chem.*, 2000, 39, 5248.
- 24 K. Y. Hwang, H. Kim, Y. S. Lee, M. H. Lee and Y. Do, *Chem. – Eur. J.*, 2009, 15, 6478.
- 25 K. D. Murugan and P. Natarajan, *Eur. Polym. J.*, 2011, 47, 1664.
- 26 A. M. Asiri, S. A. El-Daly and S. A. Khan, *Spectrochim. Acta, Part A*, 2012, 95, 679.
- 27 Q. D. Liu, W. L. Jia and S. Wang, *Inorg. Chem.*, 2005, 44, 1332.
- 28 Y. Yang, M. H. Zeng, X. H. Zhao and H. Liang, *Inorg. Chim. Acta*, 2009, 362, 3065.
- 29 X. M. Liu, X. Y. Mu, H. Xia, L. Ye, W. Gao, H. Y. Wang and Y. Mu, *Eur. J. Inorg. Chem.*, 2006, 4317.
- 30 Y. Hu, Q. Li, H. Li, Q. Guo, Y. Lua and Z. Li, *Dalton Trans.*, 2010, 39, 11344.